

# Preparing squeezed, cat and GKP states with parity measurements

Zhiyuan Lin,<sup>1,\*</sup> Sen Li,<sup>1,\*</sup> Jingyan Feng,<sup>2</sup> Valentin Ivannikov,<sup>2,†</sup> Matteo Fadel,<sup>3,‡</sup> and Tim Byrnes<sup>2,1,4,5,§</sup>

<sup>1</sup>*State Key Laboratory of Precision Spectroscopy, School of Physical and Material Sciences,  
East China Normal University, Shanghai 200062, China*

<sup>2</sup>*New York University Shanghai; NYU-ECNU Institute of Physics at NYU Shanghai,  
567 West Yangsi Road, Shanghai, 200124, China.*

<sup>3</sup>*Department of Physics, ETH Zürich, 8093 Zürich, Switzerland*

<sup>4</sup>*Center for Quantum and Topological Systems (CQTS),  
NYUAD Research Institute, New York University Abu Dhabi, UAE.*

<sup>5</sup>*Department of Physics, New York University, New York, NY 10003, USA*

(Dated: February 10, 2026)

Bosonic modes constitute a central resource in a wide range of quantum technologies, providing long-lived degrees of freedom for the storage, processing, and transduction of quantum information. Such modes naturally arise in platforms including circuit quantum electrodynamics, quantum acoustodynamics, and trapped-ion systems. In these architectures, coherent control and high-fidelity readout of the bosonic degrees of freedom are achieved via coupling to an auxiliary qubit. When operated in the strong dispersive regime, this interaction enables parity measurements of the mode which, in combination with phase-space displacements, constitute a standard experimental tool for full Wigner-function tomography. Here, we propose a protocol based on displaced parity measurements that allows for the preparation of a variety of bosonic quantum states. As a first example, we demonstrate the generation of squeezed states, achieving up to  $\sim 9$  dB of squeezing after only three parity measurements, and show that the protocol is robust against experimental imperfections. Finally, we generalize our approach to the preparation of other paradigmatic bosonic states, including cat and Gottesman–Kitaev–Preskill states.

## I. INTRODUCTION

Heisenberg’s uncertainty principle states that two canonically conjugated observables (i.e. position and momentum) have limits on the precision of their simultaneous estimate. This is formalized by stating that the product of their variances cannot be smaller than a value set by quantum mechanics. While particular types of states (e.g. coherent states) have equal uncertainties in the two observables, squeezed states reduce the uncertainty in one variable at the expenses of increasing the uncertainty in the other. This allows for a way of reducing quantum noise below the standard quantum limit, where the noise of a measurement is limited by quantum noise.

Since the first observation of squeezing [1], experimental generation is now commonplace with best squeezing levels up to 15 dB in optical systems [2, 3]. Methods of generating squeezed states include parametric processes from nonlinearities [4–9], conditional preparation based on quantum nondemolition measurements [10–13], coupling to additional modes [14–16], nonadiabatic techniques [17], and many-body dynamics [18–20]. The primary application of squeezed states is for quantum metrology, where they may be used for precision measurements [21–24], but they also play a crucial role in quantum communication [25] and simulation [26, 27].

While optical systems are canonical systems for generating squeezed states, several other platforms have demonstrated highly-controllable bosonic modes where squeezed and other quantum states can be engineered. Examples include microwave cavity modes in circuit quantum electrodynamics (cQED) [28–30], vibration modes in circuit quantum acoustodynamics (cQAD) [31], or motional states of trapped ions [32–34]. Interestingly, in these systems the bosonic mode couples to a discrete degree-of-freedom, such as a qubit, through a coupling often described by the Jaynes–Cummings model [28, 35]. The qubit can be used as the nonlinear element required to engineer effective squeezing dynamics for the bosonic mode. Specifically, squeezing is generally realized by parametric processes where the system is driven off-resonantly at suitable frequencies. The best squeezing that has been attained for these systems are 8 dB for cQED [36], around 3 dB for cQAD [31], and 5 dB in trapped ions [34]. Crucially, although methods for the measurement-based preparation of squeezed states exist, these require to measure phase-space quadratures of the bosonic state, namely to detect observables which are not easily accessible when using a qubit as measurement tool.

Squeezed states are also the building blocks for other types of states which are useful in contexts beyond quantum metrology. A paradigmatic example is the Gottesmann–Knill–Preskill (GKP) code [37], where the logical states consist of superpositions of equally displaced squeezed states. This allows for a method of forming an error protected qubit by exploiting the infinite-dimensional Hilbert space of a bosonic mode [38]. Although ideal GKP codewords have infinite energy, as they involve infinite squeezing, finite-resources approx-

\* The indicated authors are joint first authors

† valentin@nyu.edu

‡ fadelm@phys.ethz.ch

§ Corresponding author: Tim Byrnes; tim.byrnes@nyu.edu

imations are nevertheless extremely useful for a variety of applications such as quantum repeaters [39], quantum metrology [40], and error correction [41]. Approximated GKP states have been prepared on a variety of platforms, such as trapped ions [42], superconducting microwave cavities [43], and photonics [44, 45]. The primary method that is used to generate such states is “breeding” [46], where conditional displacements are performed, then interfered. While great efforts have already been devoted to its generation, the complex structure of GKP state makes challenging to generate such states, and more efficient or complementary methods are always desirable.

In this paper, we introduce methods for generating squeezed, cat, and GKP states based on displacement operations and parity measurements. We first develop a protocol for preparing squeezed states using a sequence of displaced parity measurements applied along the anti-squeezed quadrature (see Fig. 1(a)). The key observation underlying this approach is that a squeezed vacuum state occupies only the even-parity subspace of the Fock basis. In the limit of infinite squeezing, the state becomes invariant under displacements along the squeezed axis, which leads to a set of eigenvalue conditions that can be implemented through parity measurements. We analyze the performance of this scheme by quantifying the achievable squeezing and assessing the impact of realistic imperfections, demonstrating the robustness of the protocol. We further show that sequences of displacements combined with parity measurements can be interpreted as operations that generate coherent superpositions of a state and its phase-space-reflected counterpart. This observation enables a natural extension of the protocol to convert a squeezed state into a Gottesman–Kitaev–Preskill (GKP) state, which may be viewed as a comb of displaced squeezed states.

## II. PHYSICAL SYSTEM

### A. Definitions

The physical system that we consider in this paper is a single bosonic mode, which is associated to the annihilation operator  $a$  satisfying the canonical commutation relation  $[a, a^\dagger] = 1$ . This mode can represent a continuous-variable degree of freedom in different physical systems, such as microwave photons in cQED, or phonons in cQAD or trapped ions. We keep our formalism general such that it can be applied to any such platform.

The Hilbert space of a bosonic mode is spanned by Fock states, namely the states defined as

$$|n\rangle = \frac{(a^\dagger)^n}{\sqrt{n!}} |0\rangle, \quad (1)$$

where  $|0\rangle$  is the vacuum state satisfying  $a|0\rangle = 0$ . Co-

herent states are defined as

$$|\alpha\rangle = e^{-|\alpha|^2/2} e^{\alpha a^\dagger} |0\rangle = e^{-|\alpha|^2/2} \sum_{n=0}^{\infty} \frac{\alpha^n}{\sqrt{n!}} |n\rangle. \quad (2)$$

Since bosonic degrees of freedom arise from harmonic oscillators, it is natural to introduce position and momentum quadrature observables as

$$x = \frac{1}{2}(a + a^\dagger), \quad p = -\frac{i}{2}(a - a^\dagger), \quad (3)$$

such that  $[x, p] = i/2$ . These have eigenstates [25]

$$\begin{aligned} x|x_0\rangle &= x_0|x_0\rangle \\ p|p_0\rangle &= p_0|p_0\rangle, \end{aligned} \quad (4)$$

satisfying the orthogonality conditions

$$\begin{aligned} \langle x_0|x'_0\rangle &= \delta(x_0 - x'_0) \\ \langle p_0|p'_0\rangle &= \delta(p_0 - p'_0), \end{aligned} \quad (5)$$

and correspond to infinitely squeezed states with precisely defined position  $\langle x \rangle = x_0$ , or momentum  $\langle p \rangle = p_0$ , respectively. We may also consider a generalized quadrature parametrized by an angle  $\theta$  in phase space as

$$x^{(\theta)} = \frac{1}{2}(ae^{-i\theta} + a^\dagger e^{i\theta}) \quad (6)$$

with eigenstates

$$x^{(\theta)}|x_0^{(\theta)}\rangle = x_0^{(\theta)}|x_0^{(\theta)}\rangle. \quad (7)$$

Of particular relevance is the squeezed vacuum state, for which  $\langle x^{(\theta)} \rangle = 0$ , which is defined as [47]

$$|\xi\rangle = \frac{1}{\sqrt{\cosh r}} \sum_{n=0}^{\infty} (-1)^n \frac{\sqrt{(2n)!}}{2^n n!} e^{in\theta} \tanh^n r |2n\rangle, \quad (8)$$

where  $\xi = re^{i\theta}$ . This state can be understood as the action of the squeezing operator

$$S(\xi) = e^{\frac{1}{2}(\xi^* a^2 - \xi a^{\dagger 2})}, \quad (9)$$

on the vacuum state, i.e.  $|\xi\rangle = S(\xi)|0\rangle$ .

Defining the variance as

$$\text{Var}(x) = \langle x^2 \rangle - \langle x \rangle^2, \quad (10)$$

we have that the vacuum state  $|0\rangle$  has isotropic variance  $\text{Var}(x^{(0)}) = 1/4$ , while the squeezed state  $|\xi\rangle$  has  $\text{Var}(x^{(\theta)}) = 1/4(\cosh(2r) - \sinh(2r) \cos(\phi - 2\theta))$ . Along the direction defined by  $\theta = \phi/2$  the variance reads  $\min_{\theta} \text{Var}(x^{(\theta)}) = e^{-2r}/4$ , showing a reduction below the quantum noise of the vacuum state. This reduction is often quantified in decibel (dB) from the formula

$$S_{\text{dB}} = -10 \log_{10} \frac{\min_{\theta} \text{Var}(x^{(\theta)})}{\text{Var}_0(x)}. \quad (11)$$

Here, the variance  $\text{Var}(x^{(\theta)})$  is calculated with respect to the final state, while  $\text{Var}_0(x) = 1/4$  denotes the variance of the vacuum state, independent of  $\theta$ .

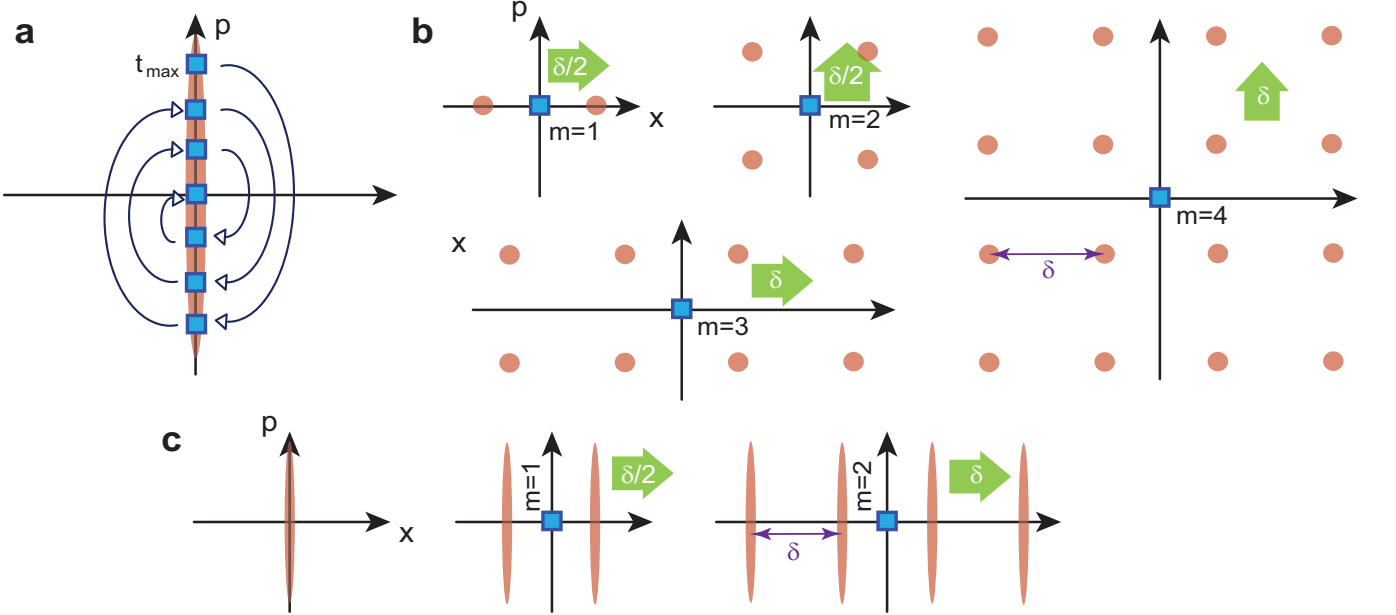


FIG. 1. Protocols for generating (a) squeezed states, (b) multi-component cat states, and (c) GKP states with parity measurements and displacements. Squares denote the displaced parity measurement  $P_+$  as given in (19), where the location of the parity measurement is at  $\alpha$ . Circles and ovals represent coherent and squeezed states respectively. Large arrows denote displacements (12), with the magnitude of the displacement indicated within the arrow, and the direction of the displacement is in the arrow direction. (a) The squeezed state measurement sequence occurs in the order indicated by the curved arrows. (b) In each measurement step, the displacement is made before the parity measurement, creating a square lattice with spacing  $\delta$ . (c) In first step, create a squeezed state using the sequence given in (a). Then use a sequence of displacements and parity measurements as shown to point reflect the squeezed state to form a comb separated by  $\delta$ .

## B. Control and measurement

We assume that the bosonic mode under investigation can be controlled and measured in some elementary ways. The main operation we consider is a displacement in phase space, as described by the operator

$$D(\alpha) = e^{\alpha a^\dagger - \alpha^* a}. \quad (12)$$

This is typically realized by driving the bosonic mode on resonance, e.g with a coherent microwave signal or laser field.

The measurement we will consider are parity measurements  $P = (-1)^n = P_+ - P_-$ , where

$$P_+ = \sum_{n \in \text{even}} |n\rangle\langle n| \quad (13a)$$

$$P_- = \sum_{n \in \text{odd}} |n\rangle\langle n| \quad (13b)$$

represent projectors into the subspaces with even/odd parity, respectively. Parity measurements are routinely performed in spin-boson systems, where the bosonic mode is coupled to a two-level (qubit) degree of freedom [28, 48–50]. In such platforms, the interaction is described by the Jaynes-Cummings model

$$H/\hbar = \omega_a a^\dagger a + \frac{\omega_0}{2} \sigma^z + g(a\sigma^+ + a^\dagger\sigma^-), \quad (14)$$

where  $\omega_a$  is the frequency of the bosonic mode,  $\omega_0$  is the frequency of the qubit, and  $g$  is the qubit-boson coupling rate. In the dispersive regime ( $\Delta \gg |g|$ ) and rotating frame of the phonon, the effective Hamiltonian reads

$$H/\hbar \approx -\frac{|g|^2}{\Delta} a^\dagger a \sigma^z \quad (15)$$

where  $\Delta = \omega_a - \omega_0$  is the qubit-boson detuning. Initializing the qubit in the state  $|+\rangle = (|0\rangle + |1\rangle)/\sqrt{2}$ , letting it interact with the mode according to the dispersive Hamiltonian for a time  $t_{\text{int}}$ , and projecting on the qubit in the  $\sigma^x$  basis results in an effective measurement of the bosonic mode that reads  $\mathcal{M}(\tau) = \mathcal{M}_+(\tau) - \mathcal{M}_-(\tau)$  [51], with  $\tau = |g|^2 t_{\text{int}}/\Delta$  and

$$\mathcal{M}_+(\tau) = \sum_n \cos(n\tau) |n\rangle\langle n| \quad (16a)$$

$$\mathcal{M}_-(\tau) = \sum_n \sin(n\tau) |n\rangle\langle n|. \quad (16b)$$

These are the projectors corresponding to measuring the qubit in the  $|\pm x\rangle$  state, respectively. For the choice  $\tau = \pi/2$ , the projectors coincide with Eqs. (13).

### III. SQUEEZING WITH PARITY MEASUREMENTS

#### A. Basic idea

Our first goal is to prepare the bosonic mode in a squeezed state by using a measurement-based state preparation protocol that relies only on displacement operations and parity measurements. To understand the idea behind our approach, we first observe that the squeezed vacuum (8) has an even parity, hence it is an eigenstate of the even parity operator

$$P_+|\xi\rangle = |\xi\rangle. \quad (17)$$

Second, for an ideal infinitely squeezed state, it is invariant under translations along the anti-squeezed axis

$$D(\alpha = -it)|x_0\rangle = e^{-i(a+a^\dagger)t}|x_0\rangle = e^{-i2x_0t}|x_0\rangle \quad (18)$$

where we used Eq. (4) and  $t$  is a real (unitless) parameter. Similar relations also hold for squeezing along other directions, but for simplicity we will consider here  $x$ -squeezed states, without loss of generality. Defining the displaced parity measurement as

$$P_\pm(\alpha) = D(\alpha)P_\pm D^\dagger(\alpha), \quad (19)$$

it follows that for displacements along the anti-squeezed axis we have

$$P_+(\alpha = it)|x_0\rangle = |x_0\rangle. \quad (20)$$

Performing multiple projections along the anti-squeezed axis thus gives

$$\prod_{m=1}^M P_+(\alpha = it_m)|x_0\rangle = |x_0\rangle. \quad (21)$$

Here,  $M$  is the number of measurements that are performed. We note that it is also possible to write this in a Hamiltonian formulation (see Appendix A).

When applied to an arbitrary initial state  $|\psi\rangle$ , the parity measurement (19) results in a projection onto the even/odd parity subspace. For non-commuting displaced-parity measurements (19), the sequence of  $M$  measurements in (21) results in a series projections onto an increasingly narrow subspace. For  $M$  sufficiently large, we expect that any initial state  $|\psi\rangle$  converges to a squeezed state.

#### B. Squeezing protocol with postselection

After having introduced the basic idea behind our squeezing protocol, we now formulate it more rigorously. Let us define the projector for a sequence of even parity projections along the desired squeezing orientation  $\theta$  as

$$\mathcal{P}_\theta(\vec{t}) = \prod_{m=1}^M P_+(\alpha = ie^{i\theta}t_m) \quad (22)$$

where  $\vec{t} = (t_1, t_2, \dots, t_M)$  is a sequence of adimensional time parameters. The order of operators in the product proceeds from right to left, such that the operator with  $t_1$  is applied first and  $t_M$  last to the state. We note that, since the measurement sequence (22) involves only the even parity outcomes, to implement this operator in practice postselection is required.

An equivalent expression for the operator (22) is

$$\mathcal{P}_\theta(\vec{t}) = D(ie^{i\theta}t_M) \left[ \prod_{m=1}^M P_+ D(-ie^{i\theta}\Delta t_m) \right] \quad (23)$$

where the difference between displacements is

$$\Delta t_m = t_m - t_{m-1}, \quad (24)$$

and we take  $t_0 = 0$ . In the above, we have used the identities for the displacement operators  $D^\dagger(\alpha) = D(-\alpha)$  and the formula for combining displacements [47]

$$D(\alpha)D(\beta) = e^{i\text{Im}(\alpha\beta^*)} D(\alpha + \beta). \quad (25)$$

Eq. (23) is simpler from an implementation standpoint, as it simplifies two consecutive displacements.

We then claim that for a suitable choice of displacements  $\vec{t}$

$$|\mathcal{P}_\theta(\vec{t})|0\rangle := \frac{|\mathcal{P}_\theta(\vec{t})|0\rangle}{\sqrt{p_{\text{suc}}(\theta, \vec{t})}} \approx |x_0^{(\theta)} = 0\rangle, \quad (26)$$

where the state that is approached is the squeezed state (7). Here we defined the success probability

$$p_{\text{suc}}(\vec{t}) = \langle 0|\mathcal{P}_\theta^\dagger(\vec{t})\mathcal{P}_\theta(\vec{t})|0\rangle. \quad (27)$$

The success probability of the  $m$ th measurement can be written as

$$p_m^{\text{suc}} = \frac{p_m^{\text{suc}}(\vec{t}_m)}{p_{\text{suc}}(\vec{t}_{m-1})} \quad (28)$$

where  $\vec{t}_m = (t_1, t_2, \dots, t_m)$  is  $\vec{t}$  truncated to the  $m$ th measurement.

Due to the probabilistic nature of the parity measurement outcomes, the performance of our protocol is highly dependent upon the choice of  $\vec{t}$ . In the next section, we show some concrete choices of  $\vec{t}$  which have a good performance in terms of generating squeezed states.

### IV. NUMERICAL EVALUATION

#### A. Method

We numerically simulate our protocol to illustrate its performances on the generation of squeezed states. To include the description of losses, which are inevitable in

experimental realizations, we express Eq. (26) in the density matrix formalism. For this, we note that each measurement step corresponds to the operation

$$\rho^{(m)} = \frac{\sum_k E_k P_+(\alpha = ie^{i\theta} t_m) \rho^{(m-1)} P_+^\dagger(\alpha = ie^{i\theta} t_m) E_k^\dagger}{\text{Tr}(P_+(\alpha = ie^{i\theta} t_m) \rho^{(m-1)} P_+^\dagger(\alpha = ie^{i\theta} t_m))}, \quad (29)$$

where  $\rho^{(m)}$  is the state after  $m$  measurements. Here we introduced the Kraus operator for bosonic loss

$$E_k = \sqrt{\frac{(1-\eta)^k}{k!}} \sqrt{\eta}^{a^\dagger a} a^k, \quad (30)$$

where  $k$  is the number of lost bosons, and  $\epsilon = 1 - \eta$  denotes the probability of losing a photon within each measurement step.

We note that the bosonic loss operator is applied after *each* measurement in Eq. (29). Thus after  $M$  measurements, there is a probability of  $1 - \eta^M$  that at least one boson has been lost. Thus for any  $\epsilon > 0$ , the probability that no error has occurred is exponentially diminishing. We choose this type of model as it is closest to experimental reality, where each measurement requires finite time to be performed.

To characterize the state resulting from our protocol, we plot its Wigner function. This is also what is typically done experimentally, using the fact that the Wigner function can be expressed as the expectation value of the displaced parity operator [52]

$$W(\alpha) = \frac{2}{\pi} \text{Tr} [\rho(P_+(\alpha) - P_-(\alpha))], \quad (31)$$

with the displaced parity operators defined in (19).

Our simulations are expressed in the Fock basis using a cutoff at  $|n_{\text{cut}}\rangle$ , where  $n_{\text{cut}}$  is chosen large enough to ensure convergence.

## B. Measurement sequence

We start discussing a suitable choice for the measurement parameters  $\vec{t}$ , which determine the measurement sequence to be performed. Through numerical observations, we decide to focus on the ansatz

$$t_m = (-1)^{m-1} t_{\text{max}} \left( 1 - \frac{\lfloor (m-1)/2 \rfloor}{\lfloor (M-1)/2 \rfloor} \right) \quad (32)$$

Here,  $\lfloor \cdot \rfloor$  is the floor function and we only consider odd  $M$ . The measurement pattern is illustrated in Fig. 1. The first measurement occurs at  $\alpha = t_{\text{max}} e^{i\theta}$ , followed by a measurement at  $\alpha = -t_{\text{max}} e^{i\theta}$ . The next two measurements are symmetrically distributed towards the origin but with smaller amplitudes, until the final measurement is at the origin.

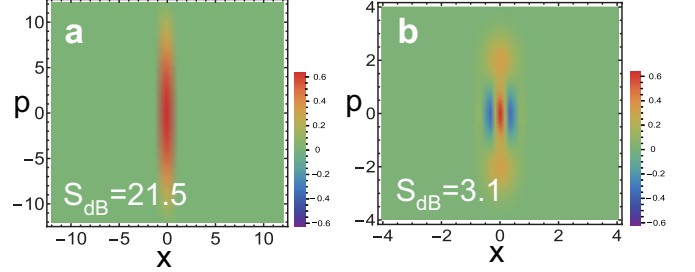


FIG. 2. Wigner functions of the squeezed state generated according to (26). We compare two measurement sequences: (a) symmetric ordering (32) and (b) linear ordering (33). Wigner functions were calculated using (31). We use  $t_{\text{max}} = 2$  and  $M = 11$  for both cases. Cutoffs of (a)  $n_{\text{cut}} = 601$  and (b)  $n_{\text{cut}} = 101$  were used.

From an intuitive point of view, the measurement sequence (32) is a reasonable choice for the following reasons. First, it ensures that the final measurement occurs at the vacuum  $t_M = 0$ , which enforces the prepared state to have an even parity. This is consistent with any squeezed state (8) and it thus maximizes the fidelity with respect to this class of states. Second, the measurements are symmetrically distributed about the origin along the anti-squeezing axis, reflecting the fact that squeezed vacuum states (8) are invariant under a rotation  $e^{i\pi a^\dagger a}$ .

We do not prove or claim that (32) is optimal; however, we have not found a superior ansatz in our numerical investigations (Fig. 2(a)). Other choices of measurement patterns always distributed along a line also produce squeezing, but can result in deviations from the target state or lower squeezing. As an example, we show in Fig. 2(b) the Wigner function for the same number of measurements and amplitude, comparing (32) and a linear sequence

$$t_n = t_{\text{max}} \left( 1 - \frac{m-1}{M-1} \right). \quad (33)$$

We see that the ansatz (32) has better performance in terms of generating a squeezed state. Henceforth, we discuss the performance within the choice (32).

## C. Convergence to an infinitely squeezed state

We first demonstrate our claim (26), where for a suitable measurement pattern the state approaches an infinitely squeezed state. Figures 2(a) and 3 shows some representative results with  $M = 11$  measurements. From Fig. 2(a) we see an excellent amount of squeezing, reaching  $S_{\text{dB}} = 21.5$  dB. In Figure 3(a), we show the Fock state amplitudes and compare it to a squeezed state with  $\xi$  chosen to most closely approximates our final state. We see a nearly indistinguishable amplitude distribution, meaning a high fidelity. Fig. 3(b) shows the success probabilities for each measurement Eq. (28). Note how the first few

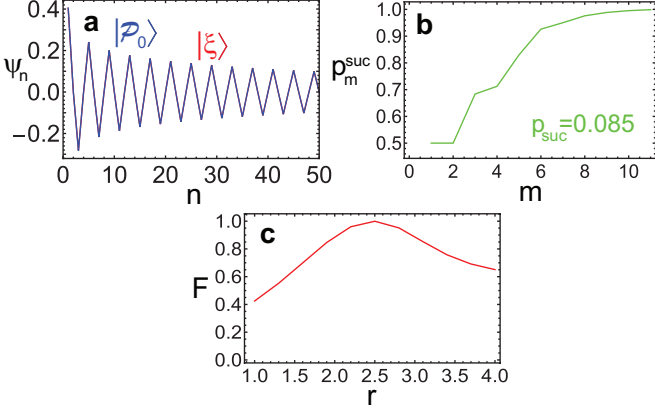


FIG. 3. Convergence of the state (26) towards the infinitely squeezed state. We use the measurement sequence (32) with  $M = 11$ ,  $t_{\max} = 2$ ,  $\theta = 0$ . (a) Wavefunction  $\psi_n = \langle n|P_0(\vec{t})\rangle$ . A comparison to the squeezed state with  $\xi = 2.5$  is shown. (b) Success probability  $p_m^{\text{suc}}$ . (c) Fidelity with squeezed states  $F = |\langle \xi = r | P_0(\vec{t}) \rangle|^2$ . We use a Fock state truncation of  $n_{\text{cut}} = 601$ .

measurements have typically  $p_m^{\text{suc}} \approx 0.5$ , but generally these converge towards  $p_m^{\text{suc}} \rightarrow 1$  as  $m$  increases. For this reason, the total success probability does not follow a simple exponential decay with  $M$ ; but it rather depends on the specific details of the sequence, including initial state and measurement points. For this example we find  $p_{\text{suc}} \approx 8.5\%$ , which is significantly better than  $1/2^M \approx 0.05\%$ . Fig. 3(c) shows the fidelity with respect to the squeezed state (8) for a range of squeezing parameters. We see that the final state is very closely approximated ( $F = 0.998$ ) by a squeezed state with  $\xi = 2.5$ .

Generally, we find that the larger the number of measurements  $M$ , the better the convergence towards the infinitely squeezed state is. The numerical limitation is however that an infinitely squeezed state has a non-negligible population of states with very high Fock number, eventually exceeding our Hilbert space truncation at  $|n_{\text{cut}}\rangle$ . To see this, set  $r \rightarrow \infty$  in (8) and we have

$$\begin{aligned} |x_0 = 0\rangle &\propto \sum_{n=0}^{\infty} (-1)^n \frac{\sqrt{(2n)!}}{2^n n!} |2n\rangle \\ &\approx \sum_{n=0}^{\infty} \frac{(-1)^n}{(\pi n)^{1/4}} |2n\rangle, \end{aligned} \quad (34)$$

which is slowly converging in Fock number. With a larger number of measurements  $M$ , the truncation effects start to play a role, effectively limiting the level of squeezing that can be obtained. For example, for  $M = 21$  measurements with  $t_{\max} = 5$  and a truncation  $n_{\text{cut}} = 1001$ , we obtain a squeezing of up to  $S_{\text{dB}} = 26$  dB. It is however likely the actual squeezing level is even larger.

#### D. Small number of measurements

Actual experimental implementations of our protocol are limited in the total number of measurements  $M$ , due to either constraints on time or tradeoff with losses. Therefore, it is of interest to know what level of squeezing can be attained for a small, finite, number of measurements. As mentioned above, in the limit of large number of measurements  $M$  the prepared state converges towards a highly squeezed state. For a few number of measurements, however, we have to deal with a dynamical regime of the protocol, before convergence. For this reason, there is a strong dependence on the choice of initial state and  $t_{\max}$ . In the following, we investigate this dependence, always considering the ideal scenario without losses. The effect of losses will then be discussed in detail in the next section.

Figure 4 shows the effect of different choices of  $t_{\max}$  for a fixed small number of measurements  $M = 3$ . In Figures 4(a)-(c), we show in the Fock basis the final states obtained from three different  $t_{\max}$ , together with the closely matching squeezed state. Importantly, we see that there is an optimal value of  $t_{\max}$  which maximizes the amount of squeezing. In fact, choices of  $t_{\max}$  that are too small result in almost no squeezing, since all projections occur near the origin in phase space. This is clear for  $t_{\max} = 0$ , where all the displaced parity measurements are simply  $P_+$  and the final result is still the vacuum state. For a choice of  $t_{\max}$  that is too large, the obtained state shows a large disagreement with the family of squeezed states, mainly due to the lack of convergence for  $M$  small. At the optimal  $t_{\max}$ , the state closely approximates a squeezed state with a large fidelity of  $F \approx 0.99$ . In Fig. 4(d) we evaluate the squeezing with (11) and we obtain a maximum value of  $S_{\text{dB}} \approx 8.9$ . The Wigner function for the optimized case is shown in Fig. 4(e), where we see the expected squeezed distribution. Some minor Wigner negativity is seen due to the finite number of measurements. The total success probability is shown in Fig. 4(g). For the optimum  $t_{\max}$ ,  $p_{\text{suc}} = 0.32$ . Thus, as long as the maximum displacement  $t_{\max}$  is optimized, even a very small number of measurements can result in the preparation of a state with a significant amount of squeezing with large success probability.

#### E. Effect of losses

In many experimental platforms of interest for our work (e.g. photonic, phononic), the dominant decoherence mechanism is energy relaxation, meaning the loss of excitations towards the environment. Hence, it is of crucial importance to investigate whether squeezing may be realized under realistic circumstances that include inevitable imperfections. To this end, we repeat the analysis presented in the previous section including losses in the dynamics, using the density matrix formulation (29).

In Fig. 4(f) we show the effect of losses on the Wigner

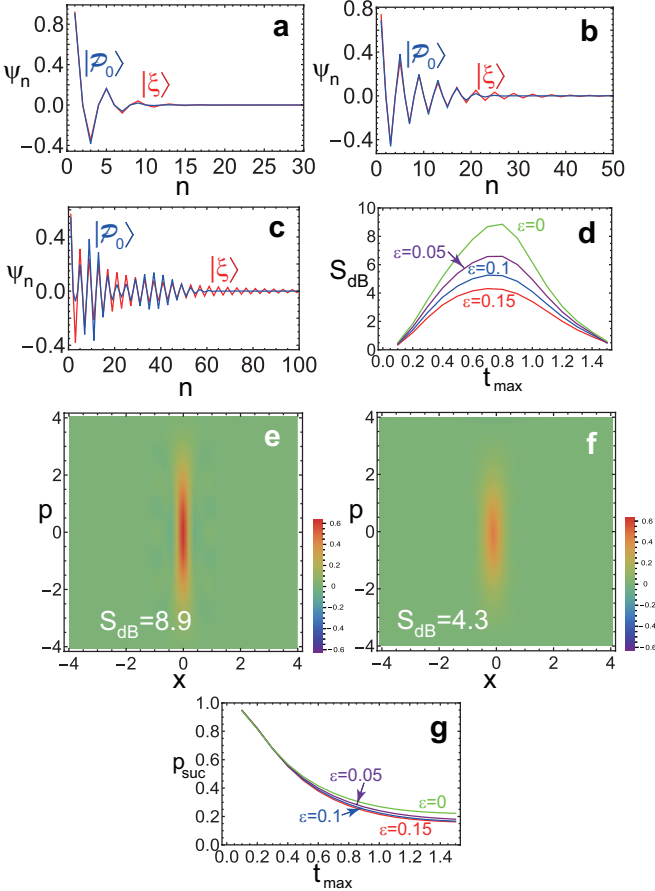


FIG. 4. Effect of the amplitude of displacement  $t_{\max}$  with a small number of measurements. We evaluate (26) with the measurement sequence (32) with  $M = 3$  and  $\theta = 0$ . Wavefunction  $\psi_n = \langle n | \rho | n \rangle$  for (a)  $t_{\max} = 0.4$ ; (b)  $t_{\max} = 0.8$ ; (c)  $t_{\max} = 1.5$ . A comparison to the squeezed state with (a)  $\xi = 0.6$ ; (b)  $\xi = 1.2$ ; (c)  $\xi = 1.8$  is shown. The success probabilities of each of the sequences is indicated in each figure. (d) The squeezing (11) as a function of  $t_{\max}$ . The Wigner distribution using the optimal  $t_{\max} = 0.8$  for (e)  $\epsilon = 0$  and (f)  $\epsilon = 0.15$ . (g) The total success probability (27) as a function of  $t_{\max}$ . The photon loss probability  $\epsilon = 1 - \eta$  are shown for (d)(e). For (a)(b)(c)(e) the photon loss probability is  $\epsilon = 0$ . We use a Fock state truncation of  $n_{\text{cut}} = 201$  for the pure state calculations and  $n_{\text{cut}} = 51$  for the mixed state calculations.

function, always for  $M = 3$  measurements. Compared to the lossless case, Fig. 4(e), it is visible that the squeezing is diminished, with a broader distribution having a lower amplitude at the origin. The squeezing reduction is also visible in Fig. 4(d), where for 15 % loss per measurement the squeezing reduces to 4.3 dB. Interestingly, the optimal value of displacement  $t_{\max}$  appears to be largely unaffected by the presence of loss. The total success probability shown in Fig. 4(g) is also largely unaffected by the presence of losses.

Figure 5 shows the effect of losses for the case of a larger number of measurements,  $M = 11$ . For the Fock

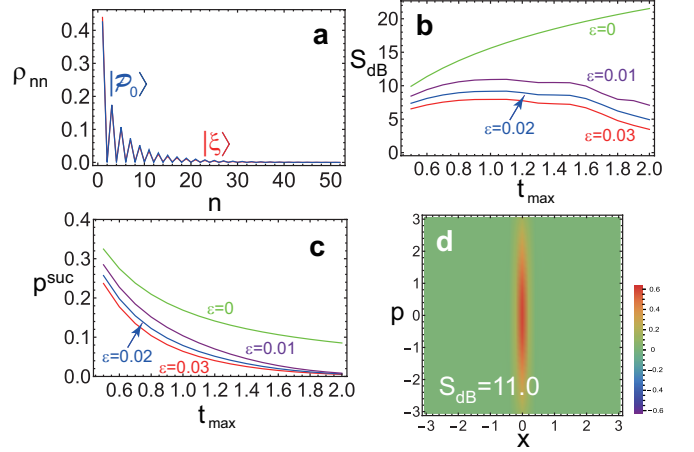


FIG. 5. Effect of bosonic loss on a larger number of measurements  $M = 11$ . (a) The diagonal density matrix elements  $\rho_{nn} = \langle n | \rho | n \rangle$  versus the Fock number for  $t_{\max} = 1.1$ ,  $\epsilon = 0.01$ . The squeezed state that is the closest match to the obtained state with  $\xi = 1.5$  is shown for comparison. (b) The attained squeezing for various  $t_{\max}$  and the loss probabilities  $\epsilon$  as shown. (c) The total success probability as a function of  $t_{\max}$  for the loss probabilities  $\epsilon$  as marked. (d) The Wigner function of the final state for  $t_{\max} = 1.1$ ,  $\epsilon = 0.01$ . For pure state ( $\epsilon = 0$ ) calculations  $n_{\text{cut}} = 601$  is used, for mixed state ( $\epsilon > 0$ ) calculations  $n_{\text{cut}} = 51$  is used.

state populations shown in Fig. 5(a), one major difference with the pure state case (see Fig. 3(a)) is that high photon numbers are suppressed. This occurs due to the bosonic amplification of losses for larger Fock number states [53, 54], which come as an advantage in numerical simulations since it allows us to set the Hilbert space truncation to a lower  $n_{\text{cut}}$  value without affecting the accuracy of the results. Evaluating the squeezing, we note that the presence of losses causes a significant drop in the squeezing level, see Fig. 5(b). This is also due to the fact that for a larger number of measurements  $M$  losses are more pronounced, since  $\epsilon$  is the loss probability *per* measurement. For example, for  $\epsilon = 0.01$ , this corresponds to a total loss probability of  $1 - \eta^M \approx 0.1$  for  $M = 11$ . The introduction of loss creates an optimal value of  $t_{\max}$  around  $t_{\max} \approx 1$ , whereas for  $\epsilon = 0$  the optimal value seems to occur outside our simulation parameter regime, for  $t_{\max} > 2$ . The total success probabilities, which we show in Fig. 5(c), are also more affected by losses compared to the case with  $M = 3$  shown in 4(g). This is because here the loss probability is higher, and thus also the probability to accidentally flip the parity of the state during the protocol. Finally, we show in Fig. 5(d) the Wigner function of the resulting state. While not attaining the impressive squeezing of the lossless case, see Fig. 5(b), considerable squeezing may still be obtained in the presence of losses.

## V. BEYOND SQUEEZED STATES

The protocol we have introduced is not limited to the measurement-based preparation of squeezed states, but it can be adjusted for the preparation of other types of states. In this section, we illustrate methods for generating multi-component Schrodinger cat states and GKP states, which play a crucial role for error-protected quantum information encoding and quantum metrology.

### A. Multi-component cat states

The key observation we take inspiration from is the fact that even/odd cat states  $|\alpha\rangle \pm |-\alpha\rangle$  can be prepared by performing parity measurements on the coherent state  $|\alpha\rangle$ . This is because a coherent state can be written as the sum of even/odd cat states with a well defined parity,  $|\alpha\rangle \simeq (|\alpha\rangle + |-\alpha\rangle) + (|\alpha\rangle - |-\alpha\rangle)$ , meaning that a parity measurement results in a projection onto one of these two cat states. More formally, we can write

$$P_{\pm}|\alpha\rangle = \frac{1}{2}(|\alpha\rangle \pm |-\alpha\rangle), \quad (35)$$

which can be verified using (2).

From a geometrical perspective, we can imagine that a parity measurement at the origin results in a point reflection around the origin, such that for a coherent state  $|\alpha\rangle$  a new coherent state  $|-\alpha\rangle$  is spawned. Therefore, by iterating displacements and parity measurements according to

$$|\mathcal{C}(\vec{\alpha})\rangle = \left[ \prod_{m=1}^M P_+ D(\alpha_m) \right] |0\rangle \quad (36)$$

various superpositions of coherent states, i.e. multi-component cat states, can be generated. Here,  $\vec{\alpha} = (\alpha_1, \alpha_2, \dots, \alpha_M)$  specifies the displacement sequence that is performed. Performing  $M$  measurements produces a superposition of up to  $2^M$  coherent state, due to each measurement doubling the number of coherent states according to Eq. (35). Note that, this is different from the squeezing sequence Eq. (22), as the displaced parity measurements involve two displacements, c.f. Eq. (19).

The result of Eq. (36) can be evaluated by combining Eq. (35) and Eq. (25). The latter equation involves a phase, coming from the Baker–Campbell–Hausdorff (BCH) formula, hence Eq. (36) will produce a superposition of coherent states which, in general, will involve nontrivial phase factors. For example, for  $M = 2$  measurements we have

$$|\mathcal{C}(\vec{\alpha})\rangle = \frac{1}{4} \left( e^{i\phi} |\alpha_1 + \alpha_2\rangle + e^{-i\phi} |\alpha_1 - \alpha_2\rangle + e^{-i\phi} |-\alpha_1 + \alpha_2\rangle + e^{i\phi} |-\alpha_1 - \alpha_2\rangle \right) \quad (37)$$

where  $\phi = \text{Im}(\alpha_2 \alpha_1^*)$ .

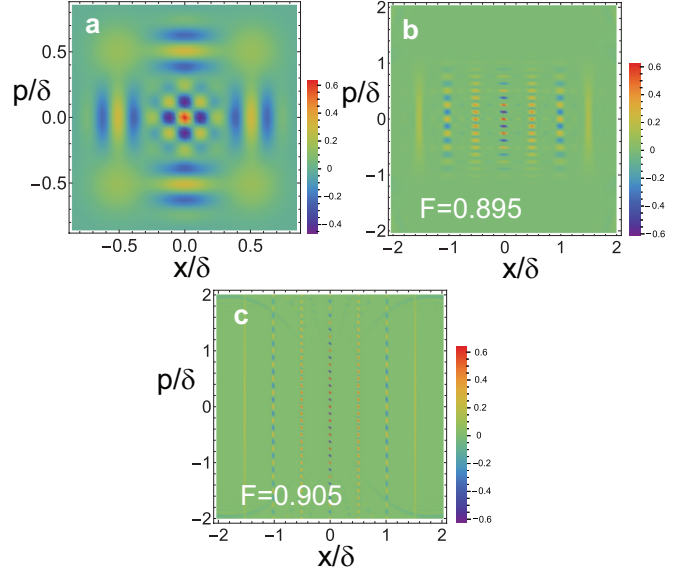


FIG. 6. Wigner functions for (a) multi-component cat states (36) and (b)(c) GKP codeword  $|1_L\rangle$  given in (42). To generate the state in (a), the sequence (36) is used with  $M = 2$  and  $\vec{\alpha} = \{\delta/2, i\delta/2\}$ . The generated state has a fidelity of  $F = 1$  with respect to the state (37) with  $\phi = 0$ . For (b), we use the same parameters as Fig. 4(e) ( $M = 3, t_{\text{max}} = 0.8, \theta = 0$ ) to generate the initial squeezed vacuum state, before applying a further  $M = 2$  measurements in (42). For (c), we use the same parameters as Fig. 2(a) ( $M = 11, t_{\text{max}} = 2, \theta = 0$ ) to generate the initial squeezed vacuum state, before applying a further  $M = 2$  measurements in (42). Fidelities comparison to the approximate GKP state (43) after optimization of  $r, \sigma_{\text{env}}$  are shown in the figures. Fock state truncation of  $n_{\text{cut}} = 201$  is used in (a)(b) and  $n_{\text{cut}} = 301$  for (c). A lattice spacing  $\delta = 2\sqrt{\pi}$  is used for all calculations.

By choosing the displacements  $\vec{\alpha}$  appropriately, some interesting states can be generated. In Figure 1(b), we show a scheme for making a square lattice of coherent states. The measurement sequence corresponds in this case to

$$\alpha_m = i \frac{1+(-1)^m}{2} 2^{\lfloor (m-1)/2 \rfloor - 1} \delta. \quad (38)$$

Each measurement doubles the lattice size, thus resulting very quickly in the creation of large lattices. Figure 6(a) shows the Wigner function for  $M = 2$  measurements. Due to the BCH phases, in order to obtain a superposition with an even phase, it is convenient to choose a lattice spacing of  $\delta = 2\sqrt{\pi}$ . Since the BCH phases can be also interpreted as a Berry phase, if the area swept out by multiple displacements is a multiple of  $2\pi$  then the phases are removed. Further phase control can be performed by using selective number dependent arbitrary phase (SNAP) methods [55]. For example, if the phase of one coherent needs to be adjusted, then it can be displaced to the vacuum, then a SNAP operation can selectively adjust the phase of the  $|0\rangle$  state.

## B. GKP states

Another paradigmatic family of states we can prepare with our protocol are Gottesmann-Knill-Preskill (GKP) states, which largely used for encoding logical qubit states into bosonic modes. The GKP codewords are defined as [37]

$$|0_L\rangle \propto \sum_{j=-\infty}^{\infty} |x_0 = 2j\sqrt{\pi}\rangle \quad (39a)$$

$$|1_L\rangle \propto \sum_{j=-\infty}^{\infty} |x_0 = (2j+1)\sqrt{\pi}\rangle. \quad (39b)$$

These are a superposition of infinitely  $x$  squeezed states with lattice spacing  $\delta = 2\sqrt{\pi}$ . Since ideal GKP codewords have infinite energy, experimental realization rely of their approximation using finitely squeezed states and an overall Gaussian envelope in the sums appearing in Eqs. (39) [46].

Following this observation, approximated GKP states may be prepared by combining our protocols for generating squeezed states and superpositions of coherent states. The protocol we propose is shown in Fig. 1(c). First, an  $x$ -squeezed vacuum state is generated using the measurement sequence (26). Then, it is displaced by half a period  $\delta/2 = \sqrt{\pi}$  and the projection  $P_+$  is performed through parity measurement. Let us remember that, according to Eq. (35), this measurement creates a point reflection of a coherent states. Since an arbitrary state  $|\psi\rangle$  can be decomposed in terms of coherent states, this creates a superposition according to

$$\begin{aligned} P_+|\psi\rangle &= \frac{1}{2\pi} \int d^2\alpha \langle\alpha|\psi\rangle (|\alpha\rangle + |-\alpha\rangle) \\ &= \frac{1}{2}(|\psi\rangle + |-\psi\rangle), \end{aligned} \quad (40)$$

where we applied the identity operator  $I = \int d^2\alpha |\alpha\rangle\langle\alpha|/\pi$  and defined

$$|-\psi\rangle := \frac{1}{\pi} \int d^2\alpha \langle\alpha|\psi\rangle |-\alpha\rangle \quad (41)$$

as the point reflected state. Hence the parity operator creates a superposition of the original state and its point reflected state. Since the  $x$ -squeezed vacuum state is symmetric around the origin, applying the sequence given in Fig. 1(c) approximately produces the GKP codeword  $|1_L\rangle$ . The state can be written as

$$|\mathcal{G}(\vec{t}, \vec{\alpha})\rangle := \left[ \prod_{m=1}^M P_+ D\left(\frac{m\delta}{2}\right) \right] |\mathcal{P}_0(\vec{t})\rangle \approx |1_L\rangle, \quad (42)$$

where the initial  $x$ -squeezed vacuum state is generated using Eq. (26).

Figure 6(b)(c) shows the Wigner function for the states resulting from Eq. (42). The two panels correspond to

states obtained by starting the protocol from either the squeezed state prepared with  $M = 3$  measurements (Fig. 6(b)), or with  $M = 11$  measurements (Fig. 6(c)), respectively. We see that the pattern characteristic of GKP states is well reproduced by our approach (c.f. Ref. [56]). The Wigner function for the  $|1_L\rangle$  GKP state is characterized by a positive distribution at  $\langle x \rangle = (2j+1)\sqrt{\pi} = (\pm\delta/2, \pm 3\delta/2, \dots)$ . Between these, there is a pattern of positive and negative peaks at  $\langle x \rangle = 2j\sqrt{\pi} = (0, \pm\delta, \dots)$ , matching the patterns seen in Fig. 6(b)(c). The higher level of squeezing for the  $M = 11$  measurement case produces a wider distribution in the  $p$ -direction as expected, but also greater squeezing in the  $x$ -direction of the lattice points in the Wigner distribution. We compare the resulting state with the approximate GKP state with a Gaussian envelope, defined as

$$|1_L, \xi, \sigma\rangle \propto \sum_{j=-\infty}^{\infty} e^{-\frac{((2j+1)\sqrt{\pi})^2}{2\sigma_{\text{env}}^2}} D((2j+1)\sqrt{\pi}) S(r)|0\rangle. \quad (43)$$

up to a normalization factor. After optimizing the parameters  $r$  and  $\sigma_{\text{env}}$  we find that the resulting states have a fidelity  $F \approx 0.99$ .

## VI. SUMMARY AND CONCLUSIONS

We have explored the use of displaced parity measurements and post-selection for the measurement-based state preparation squeezed vacuum states, multi-component cat states, and GKP states. The fundamental principle that allows for the generation of squeezed states was shown in (21), namely the fact that an infinitely squeezed state is an eigenstate of the displaced parity operator. In the ideal case, high squeezing levels of up to 21.5 dB can be obtained with a modest number of measurements ( $N = 11$ ) and reasonably high success probabilities ( $p_{\text{suc}} = 8.5\%$ ). Even for a smaller number of measurements ( $N = 3$ ), 8.9 dB of squeezing can be obtained with a high success probability ( $p_{\text{suc}} = 32\%$ ). These results are based on a parity measurement sequence we have found, which results to good approximation in squeezed states, see Fig. 1(a). Under loss, squeezing levels are reduced, but still remain considerably large under realistic experimental conditions.

Besides squeezed states, we have shown that our approach can be generalized to the preparation of other types of states, such as multi-component cat states. The key insight is that parity measurement can be considered as an operation that creates a superposition of the original and its point-reflected state. Using this basic idea, lattices of coherent states can be generated, which form the basis for the preparation of GKP states.

All the measurement sequences that were considered in this work result in a projection on the even parity subspace, hence require postselection. A way to circumvent this is to use imaginary time evolution methods [57],

which can prepare any eigenstate of a given Hamiltonian and has been shown to produce a variety of states [58, 59]. The idea here is to simulate a measurement in the energy eigenbasis of (A1) and then perform adaptive unitary operations such as to ensure that convergence in the desired ground state is obtained. While more complex than post-selection, it has the advantage that higher efficiencies can be obtained.

Since known protocols for the measurement-based preparation of squeezed states naturally rely on quadrature measurements, this make them unsuitable to be realized on cavity/circuit-QED systems, trapped ions and atoms. In these platforms, in fact, the bosonic mode is read-out through a two-level degree of freedom, making more natural to perform displaced parity measurements. Therefore, our work opens up new possibilities for state preparation in microwave and optical cavities, as well as motional states of trapped ions, atoms and solid-state oscillators.

## VII. DECLARATIONS

### A. Author Contributions

Z.L. and S.L. contributed equally to this work. Z.L. and S.L. developed the theoretical framework and performed the numerical simulations. J.F. and V.I. assisted with numerical analysis and validation. M.F. and T.B. supervised the project and provided conceptual guidance. Z.L. and S.L. wrote the initial draft of the manuscript. All authors discussed the results and reviewed the manuscript.

### B. Competing Interests

The authors declare no competing interests.

## ACKNOWLEDGMENTS

This work is supported by the SMEC Scientific Research Innovation Project (2023ZKZD55); the National Natural Science Foundation of China (92576102); the Science and Technology Commission of Shanghai Municipality (22ZR1444600); the NYU Shanghai Boost Fund; the China Foreign Experts Program (G2021013002L); the NYU-ECNU Institute of Physics at NYU Shanghai; the NYU Shanghai Major-Grants Seed Fund; and Tamkeen under the NYU Abu Dhabi Research Institute grant CG008. M.F. was supported by the Swiss National Science Foundation Ambizione Grant No. 208886, and by The Branco Weiss Fellowship – Society in Science, administered by the ETH Zürich.

### Appendix A: Hamiltonian for infinitely squeezed state

An alternative formulation of the infinitely squeezed state is as the ground state of the Hamiltonian

$$H = - \sum_{n=1}^N P_+(\alpha = it_n). \quad (\text{A1})$$

It is guaranteed that  $|x_0\rangle$  is the ground state given that the eigenspectrum of (A1) is within the range  $[-N, N]$  since each term within the sum takes a value  $[-1, 1]$  for any expectation value. The eigenvalue of  $|x_0\rangle$  is  $-N$  which shows that it is the minimum value within the allowed range, showing it must be a ground state.

---

[1] G. Breitenbach, S. Schiller, and J. Mlynek, Measurement of the quantum states of squeezed light, *Nature* **387**, 471 (1997).

[2] H. Vahlbruch, M. Mehmet, K. Danzmann, and R. Schnabel, Detection of 15 dB squeezed states of light and their application for the absolute calibration of photoelectric quantum efficiency, *Physical review letters* **117**, 110801 (2016).

[3] A. Schönbeck, F. Thies, and R. Schnabel, 13 dB squeezed vacuum states at 1550 nm from 12 mw external pump power at 775 nm, *Optics letters* **43**, 110 (2017).

[4] R. Slusher, L. Hollberg, B. Yurke, J. Mertz, and J. Valley, Observation of squeezed states generated by four-wave mixing in an optical cavity, *Physical review letters* **55**, 2409 (1985).

[5] M. Banaee and J. F. Young, Squeezed state generation in photonic crystal microcavities, *Optics Express* **16**, 20908 (2008).

[6] M. Stefszky, C. M. Mow-Lowry, K. McKenzie, S. Chu, B. C. Buchler, T. Symul, D. E. McClelland, and P. K. Lam, An investigation of doubly-resonant optical parametric oscillators and nonlinear crystals for squeezing, *Journal of Physics B: Atomic, Molecular and Optical Physics* **44**, 015001 (2011).

[7] H. Nadgaran, M. A. Izadi, and R. Nouroozi, Squeezed states generation by nonlinear plasmonic waveguides: a novel analysis including loss, phase mismatch and source depletion, *Scientific Reports* **13**, 1075 (2023).

[8] C. Eichler, D. Bozyigit, C. Lang, M. Baur, L. Steffen, J. M. Fink, S. Filipp, and A. Wallraff, Observation of two-mode squeezing in the microwave frequency domain, *Physical Review Letters* **107**, 113601 (2011).

[9] B. Yurke, L. Corruccini, P. Kaminsky, L. Rupp, A. Smith, A. Silver, R. Simon, and E. Whitaker, Observation of parametric amplification and

deamplification in a josephson parametric amplifier, *Physical Review A* **39**, 2519 (1989).

[10] G. Colangelo, F. M. Ciurana, L. C. Bianchet, R. J. Sewell, and M. W. Mitchell, Simultaneous tracking of spin angle and amplitude beyond classical limits, *Nature* **543**, 525 (2017).

[11] O. Hosten, N. J. Engelsen, R. Krishnakumar, and M. A. Kasevich, Measurement noise 100 times lower than the quantum-projection limit using entangled atoms, *Nature* **529**, 505 (2016).

[12] Z. Chen, J. G. Bohnet, S. R. Sankar, J. Dai, and J. K. Thompson, Conditional spin squeezing of a large ensemble via the vacuum rabi splitting, *Physical review letters* **106**, 133601 (2011).

[13] M. H. Schleier-Smith, I. D. Leroux, and V. Vuletić, States of an ensemble of two-level atoms with reduced quantum uncertainty, *Physical review letters* **104**, 073604 (2010).

[14] D. J. Wineland, J. J. Bollinger, W. M. Itano, F. Moore, and D. J. Heinzen, Spin squeezing and reduced quantum noise in spectroscopy, *Physical Review A* **46**, R6797 (1992).

[15] M. Aspelmeyer, T. J. Kippenberg, and F. Marquardt, Cavity optomechanics, *Reviews of Modern Physics* **86**, 1391 (2014).

[16] I. D. Leroux, M. H. Schleier-Smith, and V. Vuletić, Implementation of cavity squeezing of a collective atomic spin, *Physical Review Letters* **104**, 073602 (2010).

[17] L. Xin, M. Barrios, J. T. Cohen, and M. S. Chapman, Long-lived squeezed ground states in a quantum spin ensemble, *Physical Review Letters* **131**, 133402 (2023).

[18] T. Berrada, S. Van Frank, R. Bücker, T. Schumm, J.-F. Schaff, and J. Schmiedmayer, Integrated Mach-Zehnder interferometer for Bose-Einstein condensates, *Nature communications* **4**, 2077 (2013).

[19] H. Strobel, W. Muessel, D. Linnemann, T. Zibold, D. B. Hume, L. Pezzè, A. Smerzi, and M. K. Oberthaler, Fisher information and entanglement of non-gaussian spin states, *Science* **345**, 424 (2014).

[20] B. Lücke, J. Peise, G. Vitagliano, J. Arlt, L. Santos, G. Tóth, and C. Klempert, Detecting multiparticle entanglement of Dicke states, *Physical review letters* **112**, 155304 (2014).

[21] V. Giovannetti, S. Lloyd, and L. Maccone, Advances in quantum metrology, *Nature photonics* **5**, 222 (2011).

[22] L. Pezzè, A. Smerzi, M. K. Oberthaler, R. Schmied, and P. Treutlein, Quantum metrology with nonclassical states of atomic ensembles, *Reviews of Modern Physics* **90**, 035005 (2018).

[23] T. Byrnes and E. O. Ilo-Okeke, *Quantum atom optics: Theory and applications to quantum* (Cambridge university press, 2021).

[24] M. Jabir, R. Dawkins, J. Sabines-Chesterking, D. V. Reddy, A. Lita, A. Battou, and T. Gerrits, Quantum enhanced precision metrology for quantum networks, in *Quantum 2.0* (Optica Publishing Group, 2024) pp. QTh4C-5.

[25] S. L. Braunstein and P. van Loock, Quantum information with continuous variables, *Rev. Mod. Phys.* **77**, 513 (2005).

[26] A. P. Lund, A. Laing, S. Rahimi-Keshari, T. Rudolph, J. L. O'Brien, and T. C. Ralph, Boson sampling from a gaussian state, *Phys. Rev. Lett.* **113**, 100502 (2014).

[27] C. S. Hamilton, R. Kruse, L. Sansoni, S. Barkhofen, C. Silberhorn, and I. Jex, Gaussian boson sampling, *Phys. Rev. Lett.* **119**, 170501 (2017).

[28] A. Blais, A. L. Grimsmo, S. M. Girvin, and A. Wallraff, Circuit quantum electrodynamics, *Reviews of Modern Physics* **93**, 025005 (2021).

[29] P.-B. Li and F.-L. Li, Engineering squeezed states of microwave radiation with circuit quantum electrodynamics, *Physical Review A—Atomic, Molecular, and Optical Physics* **83**, 035301 (2006).

[30] A. Krasnok, P. Dhakal, A. Fedorov, P. Frigola, M. Kelly, and S. Kutsaev, Superconducting microwave cavities and qubits for quantum information systems, *Applied Physics Reviews* **11**, <https://doi.org/10.1063/5.0155213> (2024).

[31] S. Marti, U. von Lüpke, O. Joshi, Y. Yang, M. Bild, A. Omahen, Y. Chu, and M. Fadel, Quantum squeezing in a nonlinear mechanical oscillator, *Nature Physics* **20**, 1448 (2024).

[32] F. Wolf, C. Shi, J. C. Heip, M. Gessner, L. Pezzè, A. Smerzi, M. Schulte, K. Hammerer, and P. O. Schmidt, Motional Fock states for quantum-enhanced amplitude and phase measurements with trapped ions, *Nature communications* **10**, 2929 (2019).

[33] Z. Jia, Y. Wang, B. Zhang, J. Whitlow, C. Fang, J. Kim, and K. R. Brown, Determination of multi-mode motional quantum states in a trapped ion system, *Physical Review Letters* **129**, 103602 (2022).

[34] R. T. Sutherland, S. Burd, D. Slichter, S. Libby, and D. Leibfried, Motional squeezing for trapped ion transport and separation, *Physical review letters* **127**, 083201 (2021).

[35] D. Leibfried, R. Blatt, C. Monroe, and D. Wineland, Quantum dynamics of single trapped ions, *Rev. Mod. Phys.* **75**, 281 (2003).

[36] R. Dassonneville, R. Assouly, T. Peronne, A. Clerk, A. Bienfait, and B. Huard, Dissipative stabilization of squeezing beyond 3 dB in a microwave mode, *PRX Quantum* **2**, 020323 (2021).

[37] D. Gottesman, A. Kitaev, and J. Preskill, Encoding a qubit in an oscillator, *Physical Review A* **64**, 012310 (2001).

[38] A. J. Brady, A. Eickbusch, S. Singh, J. Wu, and Q. Zhuang, Advances in bosonic quantum error correction with Gottesman–Kitaev–Preskill codes: Theory, engineering and applications, *Progress in Quantum Electronics* **93**, 100496 (2024).

[39] F. Rozpedek, K. Noh, Q. Xu, S. Guha, and L. Jiang, Quantum repeaters based on concatenated bosonic and discrete-variable quantum codes, *npj Quantum Information* **7**, 102 (2021).

[40] C. H. Valahu, M. P. Stafford, Z. Huang, V. G. Matsos, M. J. Millican, T. Chalermpusitarak, N. C. Menicucci, technblgymbes, B. Q. Baragiola, and T. R. Tan, Quantum-enhanced multiparameter sensing in a single mode, *Science Advances* **11**, eadw9757 (2025).

[41] B. Royer, S. Singh, and S. M. Girvin, Encoding qubits in multimode grid states, *PRX Quantum* **3**, 010335 (2022).

[42] C. Flühmann, T. L. Nguyen, M. Marinelli, V. Negnevitsky, K. Mehta, and J. Home, Encoding a qubit in a trapped-ion mechanical oscillator, *Nature* **566**, 513 (2019).

[43] P. Campagne-Ibarcq, A. Eickbusch, S. Touzard, E. Zalys-Geller, N. E. Frattini, V. V. Sivak, P. Reinhold, S. Puri, S. Shankar, R. J. Schoelkopf, *et al.*, Quantum error correction of a qubit encoded in grid states of an oscillator, *Nature* **584**, 368 (2020).

[44] S. Konno, W. Asavanant, F. Hanamura, H. Nagayoshi, K. Fukui, A. Sakaguchi, R. Ide, F. China, M. Yabuno, S. Miki, *et al.*, Logical states for fault-tolerant quantum computation with propagating light, *Science* **383**, 289 (2024).

[45] M. Larsen, J. Bourassa, S. Kocsis, J. Tasker, R. Chadwick, C. González-Arciniegas, J. Hastrup, C. Lopetegui-González, F. Miatio, A. Motamed, *et al.*, Integrated photonic source of Gottesman–Kitaev–Preskill qubits, *Nature* , 1 (2025).

[46] D. J. Weigand and B. M. Terhal, Generating grid states from Schrödinger-cat states without postselection, *Physical Review A* **97**, 022341 (2018).

[47] C. C. Gerry and P. L. Knight, *Introductory quantum optics* (Cambridge university press, 2023).

[48] L. G. Lutterbach and L. Davidovich, Method for direct measurement of the wigner function in cavity qed and ion traps, *Phys. Rev. Lett.* **78**, 2547 (1997).

[49] B. Vlastakis, G. Kirchmair, Z. Leghtas, S. E. Nigg, L. Frunzio, S. M. Girvin, M. Mirrahimi, M. H. Devoret, and R. J. Schoelkopf, Deterministically encoding quantum information using 100-photon Schrödinger cat states, *Science* **342**, 607 (2013).

[50] U. Von Lüpke, Y. Yang, M. Bild, L. Michaud, M. Fadel, and Y. Chu, Parity measurement in the strong dispersive regime of circuit quantum acoustodynamics, *Nature Physics* **18**, 794 (2022).

[51] J. Feng, M. Zhang, M. Fadel, and T. Byrnes, Quantum teleportation of cat states with binary-outcome measurements, *Quantum Science and Technology* **10**, 045022 (2025).

[52] A. Royer, Wigner function as the expectation value of a parity operator, *Physical Review A* **15**, 449 (1977).

[53] M. O. Scully and A. A. Svidzinsky, The super of superradiance, *Science* **325**, 1510 (2009).

[54] T. Byrnes, K. Yan, and Y. Yamamoto, Accelerated optimization problem search using Bose–Einstein condensation, *New Journal of Physics* **13**, 113025 (2011).

[55] R. W. Heeres, P. Reinhold, N. Ofek, L. Frunzio, L. Jiang, M. H. Devoret, and R. J. Schoelkopf, Implementing a universal gate set on a logical qubit encoded in an oscillator, *Nature communications* **8**, 94 (2017).

[56] J. Lee, S. Omkar, Y. S. Teo, S.-H. Lee, H. Kwon, M. Kim, and H. Jeong, Photonic hybrid quantum computing, arXiv preprint arXiv:2510.00534 <https://doi.org/10.48550/arXiv.2510.00534> (2025).

[57] Y. Mao, M. Chaudhary, M. Kondappan, J. Shi, E. O. Ilo-Okeke, V. Ivannikov, and T. Byrnes, Measurement-based deterministic imaginary time evolution, *Phys. Rev. Lett.* **131**, 110602 (2023).

[58] M. Kondappan, M. Chaudhary, E. O. Ilo-Okeke, V. Ivannikov, and T. Byrnes, Imaginary-time evolution with quantum nondemolition measurements: Multiqubit interactions via measurement nonlinearities, *Physical Review A* **107**, 042616 (2023).

[59] T. Chen and T. Byrnes, Efficient preparation of the AKLT state with measurement-based imaginary time evolution, *Quantum* **8**, 1557 (2024).